Plasma Sources Science and Technology

PAPER

Theoretical study of electron-induced vibrational excitation of NO_2

IOP Publishing Plasma Sources Science and Technology
Plasma Sources Sci. Technol. **28** (2019) 105017 (8pp) https://doi.org/10.1088/1361-6595/ab4b8a

Theoretical study of electron-induced vibrational excitation of NO_2

Hainan Liu[1], Samantha Fonseca dos Santos[2], Chi Hong Yuen[3], Pietro Cortona[1], Viatcheslav Kokoouline[3] and Mehdi Ayouz[4]

[1] Laboratoire SPMS, CNRS-UMR8580, CentralSupélec, Université Paris-Saclay, F-91190, Gif-sur-Yvette, France
[2] Department of Physics, Rollins College, Winter Park, FL 32789, United States of America
[3] Department of Physics, University of Central Florida, Orlando, FL 32816, United States of America
[4] Laboratoire LGPM, CentralSupélec, Université Paris-Saclay, F-91190, Gif-sur-Yvette, France

E-mail: mehdi.ayouz@centralesupelec.fr

Received 28 June 2019, revised 8 September 2019
Accepted for publication 7 October 2019
Published 29 October 2019

Abstract

In this study, we compute cross sections for vibrational excitation of $NO_2(X\,^2A_1)$ by electron impact. Calculations are performed using a theoretical approach based on a combination of the normal mode approximation for vibrational states of the target molecule, fixed-nuclei electron-NO_2 scattering matrices and the vibrational frame transformation employed to evaluate the scattering matrix for vibrational transitions. Thermally-averaged rate coefficients are derived from the obtained cross sections for temperatures in the 10–10000 K interval for excitation of each normal mode of the target molecule. Analytical fits for the rate coefficients for singlets and triplets are provided. In addition, a comprehensive set of calculations are performed for assessing the uncertainty of the present calculations. The uncertainty assessments indicate that the computed observables for vibrational (de-)excitation is reasonable for later use in NO_2-containing plasma kinetics modeling.

Keywords: non-equilibrium plasmas, electron-NO_2 collisions, vibrational excitation, vibrational frame transformation, molecular *R*-matrix

1. Introduction

The nitrogen dioxide (NO_2) molecule has a number of applications in engineering and science. For instance, it is used in the sterilization of medical instruments [1]. In atmospheric science, the chemiluminescent emission from electronically excited NO_2 in the O + NO reaction, known as 'air afterglow' [2], is important for understanding the complex physical processes in the middle and upper atmosphere. However, nitrogen dioxide is an undesirable pollutant in the troposphere. Exposure to the environment where the concentration of NO_2 exceeds 3 ppm for longer than 8 h (or >5 ppm for longer than 15 min) yields the adverse effect on the human respiratory system [3]. The role of this trace constituent of atmosphere constantly increases along with an increase in its emission rate caused mainly by human activities such as automobile exhaust and industrial combustion. Non-equilibrium plasma technology has been introduced over the past several years as a promising technique for NO_2 removal. The development of the technology requires knowledge of physical and chemical processes taking place in NO_2 plasma. Especially important processes are collisions between electrons and NO_2 molecules because the availability of accurate data for these process is crucial for plasma modeling.

Electron collisions with the NO_2 molecule have been extensively investigated in the past, with first studies focused on the NO_2 ionization [4–6] due to a variety of applications in plasma technology. In more recent studies, other processes in the e^-–NO_2 collisions were studied. For example, Szmytkowski *et al* [7] measured absolute total cross sections for electron-NO_2 collisions in a linear transmission experiment for the interval 0.6–220 eV of collision energies. A further investigation from intermediate to high energies was carried out by Zecca *et al* [8]. Experiments by Fox [9] and Rangwala *et al* [10] reported dissociative electron attachment (DEA) to NO_2 as a mechanism on negative-ion formation. Munjal *et al* [11] reported theoretical data on elastic integral, differential, momentum transfer cross sections, as well as electronic-excitation cross sections from the

Table 1. Structure and vibrational frequencies of NO_2 obtained in this study and compared with experimental data from [16]. ω_1, ω_2 and ω_3 are the frequencies of bending mode, symmetric stretching mode and asymmetric stretching mode, respectively.

	Bond (Å)	Angle (degrees)	ω_1 (cm^{-1})	ω_2 (cm^{-1})	ω_3 (cm^{-1})
This work	1.204	133.95	756.66	1319.21	1625.86
Exp.	1.193	134.10	750.00	1318.00	1618.00

ground electronic state to the five lowest electronically excited states of NO_2.

Despite these efforts, still now little information is available on the electron-impact vibrational excitation (VE) of NO_2. This process plays an important role in the chemistry and the physics of molecular plasma because vibrationally excited NO_2 react differently, compared to the ground-state NO_2, with other species present in the plasma [12]. To the best of our knowledge, there exist only one measurement on VE cross sections for energies 0.3–2.5 eV by Benoit and Abouaf [13]. No theoretical study on VE of NO_2 has been reported until now. As excitation of different modes have almost the same fundamental frequencies cannot be separated experimentally at least by the conventional technique, the theoretical treatment for the VE of NO_2 is indeed necessary. To fill this void, the objective of the present study is to provide VE cross sections and corresponding thermally-averaged rate coefficients obtained theoretically. Systematic calculations were performed for the excitation of the 3 lowest excited vibrational levels in the ground electronic state of NO_2. For higher vibrational states, processes such as DEA become more predominant than VE.

The paper is organized as follows. In the next section, the theoretical approach used in the present calculation is described. In section 3, the obtained VE cross sections and corresponding rate coefficients are shown and discussed. Section 4 presents uncertainty estimations of the present approach. The concluding remarks are given in section 5.

2. Theoretical approach

2.1. The properties of the NO_2 molecule and the scattering calculations

NO_2 is an open-shell molecule belonging to the C_{2v} point group at its equilibrium, with the ground state electronic configuration

$$X\,^2A_1\colon\ 1a_1^2 2a_1^2 1b_2^2 3a_1^2 2b_2^2 4a_1^2 5a_1^2 3b_2^2 1b_1^2 4b_2^2 1a_2^2 6a_1^1.$$

It is characterized by three normal modes of vibration: bending, symmetric stretching, and asymmetric stretching. Displacements along the bending and symmetric stretching modes do not break the C_{2v} symmetry of the molecule, while the asymmetric stretching mode reduces the symmetry to the C_s group.

Electronic structure and frequencies of normal modes are determined using the *ab initio* quantum chemistry package MOLPRO [14]. In the *ab initio* calculations we first performed an optimization by the complete active space self-consistent field (CASSCF) method with Hartree–Fock (HF) orbitals. The 3 core orbitals are frozen in the calculation, while the remaining 17 electrons are distributed over the active space including seven a_1, two b_1, five b_2, and one a_2 orbitals. The correlation consistent polarized valence triple zeta (`cc-pVTZ`) [15] basis set is used for all the atoms.

The frequencies of the normal modes were computed using the same model. Table 1 summarizes the optimized geometry and vibrational frequencies obtained in the present calculation and compares the results with the available experimental data.

As the table demonstrates, the present results match excellently with the experiment. From the results of the frequencies calculations, we also obtained the transformation matrix between the normal and Cartesian coordinates. The matrix is needed to generate geometries input data for electron-NO_2 scattering calculations.

The electron-scattering calculations for several values of normal coordinates were carried out using the UK *R*-matrix code [17] with the Quantemol-N interface [18]. The NO_2 target molecule in the ground electronic state is described using the `cc-pVTZ` basis set and the complete active space configuration interaction (CAS-CI) method built on orbitals obtained from the same CASSCF calculation in MOLPRO. To make the dynamical *R*-matrix calculation tractable, we freeze 10 electrons in the core $1a_1$, $2a_1$, $3a_1$, $1b_2$, $2b_2$, while the remaining 13 electrons are kept free in the active space of the $4a_1$, $5a_1$, $3b_2$, $1b_1$, $4b_2$, $1a_2$, $6a_1$, $7a_1$, $2b_1$, $5b_2$ molecular orbitals. We used an *R*-matrix sphere of radius 14 bohr, large enough to envelop the entire charge clouds of all the target electronic states included in the calculation. A partial waves expansion is used with continuum Gaussian-type orbitals up to $l \leqslant 4$. Twenty-one target states below 12 eV are retained in the final close-coupling calculation.

An accurate description of the target molecule is crucial in this model. Figure 1 displays the potential energy surface of the ground state of NO_2 computed with the *R*-matrix code, where the surface is plotted along the three normal modes and compared with the harmonic potential energy. Almost no anharmonic contribution is observed for the bending (panel (a) in the figure) and asymmetric stretching (panel (c)) modes. However, the potential energy of the symmetric stretching mode is slightly anharmonic as evident from panel (b) in the figure.

The dipole moment of NO_2 obtained in this model is 0.317 D, which is in remarkably good agreement with the experimental value of 0.316 D [19]. In the *R*-matrix calculations, we also obtain the reactance matrix (*K*-matrix) for the e^-–NO_2 collisions for all four irreducible representations

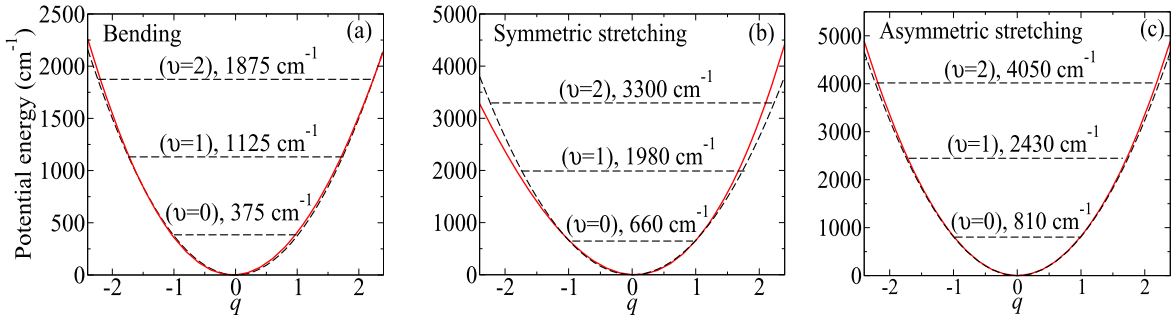

Figure 1. Potential energy curves for the ground electronic state of NO_2 as a function of the (a) bending; (b) symmetric stretching; (c) asymmetric stretching modes. The abscissa axes in the figure represent dimensionless normal coordinates. In each panel, only one mode is varied, while the other modes are kept fixed at their equilibrium positions. Red solid curves are the actual potential energies obtained from the UKRmol suite, while black dashed curves represent energies calculated in the harmonic approximation. Horizontal dashed lines denote energies of vibrational states.

(irrep) A_1, B_1, B_2 and A_2. The fixed-nuclei reactance matrices are then used to compute scattering matrices numerically according to

$$\hat{S} = \frac{\hat{1} + i\hat{K}}{\hat{1} - i\hat{K}}, \tag{1}$$

where $\hat{1}$ is the identity matrix.

2.2. Vibrational (de-)excitation cross section formula

The goal of the study is to obtain cross sections for electron-impact vibrational transitions

$$e^- + NO_2(\upsilon_i) \rightarrow e^- + NO_2(\upsilon_i'), \tag{2}$$

where the quantum number υ_i and υ_i' stand for the initial and final vibrational state of the target for normal mode i. The reaction channel for which $\upsilon_i = \upsilon_i'$ corresponds to elastic scattering. Taking an average over initial rotational states and a sum over final rotational states in the process, i.e. neglecting the rotational structure of the molecule, the cross section for VE of the mode i is expressed as

$$\sigma_{\upsilon_i'\upsilon_i}(E_{\rm el}) = \frac{\pi\hbar^2}{2mE_{\rm el}} |S_{\upsilon_i'\upsilon_i} - \delta_{\upsilon_i'\upsilon_i}|^2, \tag{3}$$

where $E_{\rm el}$ is the energy of the incident electron and m is the mass of electron. The computation of the scattering matrix $S_{\upsilon_i'\upsilon_i}$ for VE relies on the vibrational frame transformation [20]

$$S_{\upsilon_i'\upsilon_i} = \sum_{l'\lambda',l\lambda} \langle \chi_{\upsilon_i'} | S_{l'\lambda',l\lambda}(\boldsymbol{q}) |\ \chi_{\upsilon_i}\rangle \tag{4}$$

where l is the angular momentum of electron and λ is its projection on a body-fixed axis, χ_{υ_i} and $\chi_{\upsilon_i'}$ are the initial and final vibrational wave functions of the target molecule, respectively, and $\boldsymbol{q}$ denotes collectively the dimensionless normal coordinates of the molecule. $S_{l'\lambda',l\lambda}$ is an element of the fixed-nuclei scattering matrix for electron-NO_2 collisions with initial channel $l\lambda$ and exit channel $l'\lambda'$. The summation in equation (4) is achieved over all partial waves. The Gaussian–Legendre quadrature with 10 points is used to compute the integral in equation (4) numerically.

The vibrational frame transformation treatment becomes feasible, at least in principle, only if the elements of the fixed-nuclei S-matrix for the $e^- - NO_2$ system are smooth with respect to the incident energy. Therefore, the treatment is not appropriate if there are low-energy resonances in the $e^- - NO_2$ spectrum at low energies. In an attempt to analyze the behavior of S-matrix elements, we computed the absolute value squared $|S_{l'\lambda',l\lambda}|^2$ of the matrix elements as a function of the electron scattering energy at the equilibrium geometry. Figure 2 gives an idea about couplings between different partial waves in the scattering process. Here, singlet states are chosen as an example. Although five partial waves is included in the computation, only couplings between channels with $\Delta l < 2$ are not negligible for inelastic scattering. The contribution from the $\Delta l \geqslant 2$ couplings is very small. Notably, the $|S_{l'\lambda',l\lambda}|^2$ coupling producing the dominant contribution to the inelastic process for each symmetry depends only weakly on the scattering energy, as shown in figure 3. Therefore, it is reasonable to employ the vibrational frame transformation for the VE calculations.

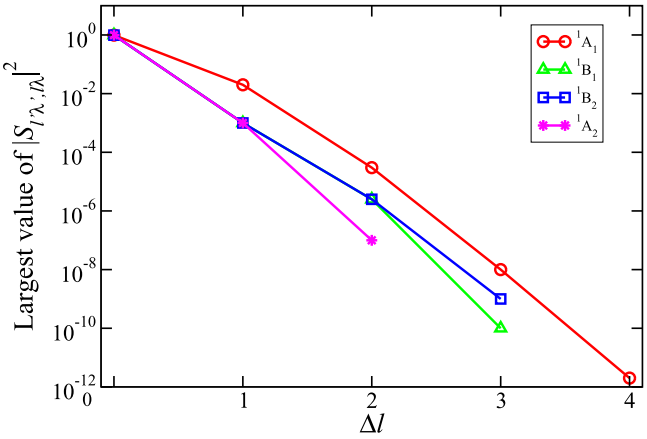

Figure 2. The largest value of $|S_{l'\lambda',l\lambda}|^2$ with respect to all possible allowed combinations of $l\lambda$, $l'\lambda'$ as a function of the difference $\Delta l = l' - l$ for all four singlet irreps of the e^-–NO_2 complex. The lowest value of l is 0 for $^1A_1$, 1 for $^1B_1$ and $^1B_2$, 2 for $^1A_2$. For $^1A_1$ (solid red line with circles), the couplings between the s and f, s and g partial waves are very small. For $^1B_1$ (solid green line with triangles) and $^1B_2$ (solid blue line with squares), since s-wave scattering is forbidden by symmetry, only couplings between p, d, f and g partial waves is shown. For $^1A_2$ (solid pink line with stars), s and p partial waves scattering is not allowed.

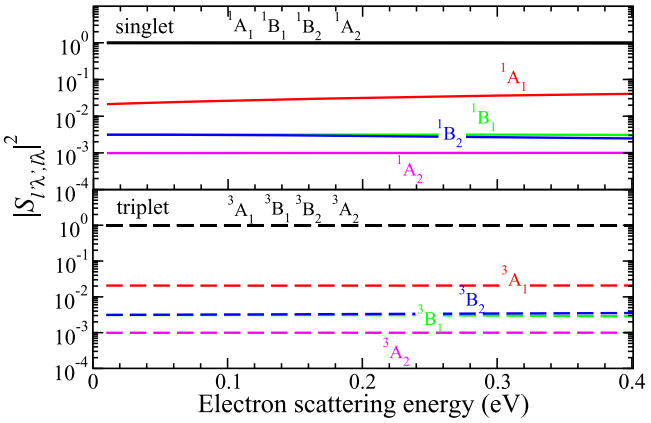

Figure 3. The figures shows dominant (absolute value squared) elements $|S_{l'\lambda',l\lambda}|^2$ of the scattering matrix as a function of the electron scattering energy at the NO_2 equilibrium. Black lines: coupling between channels with $\Delta l = 0$. Color lines: coupling between channels with $\Delta l = 1$.

3. Cross sections and rate coefficients

In this section, we present the calculated cross sections and rate coefficients for vibrational (de-)excitation of NO_2 for collision energies below the first resonance <1.6 eV of the $^3B_1$ symmetry. The VE cross sections for changing up to two quanta are obtained for the three vibrational modes. For the symmetric stretching mode, the results for the double-quantum transition should be viewed as not very accurate, because the normal mode approximation is poor for the symmetric stretching mode as discussed above.

Figure 4 displays the VE cross sections for the singlet and triplet states of the e^-–NO_2 complex with the target molecule being initially in the ground vibrational level.

Not surprisingly, the $1 \leftarrow 0$ cross sections of the e^-–NO_2 singlet complex (solid red curves) are the largest compared to the triplet and $2 \leftarrow 0$ transitions. The $1 \leftarrow 0$ VE cross section for triplet (dashed red curve) bending mode has the same shape as that of the singlet. Its magnitude is smaller than that for the singlet by more than a factor of 4. For the symmetric stretching mode (see figure 4(b)), the $1 \leftarrow 0$ VE cross sections for both singlet and triplet depend very weakly on the scattering energy up to 0.6 eV. Note that the $1 \leftarrow 0$ VE cross sections for the asymmetric stretching mode are zero due to the symmetry of the scattering matrix with respect to positive and negative values of displacements along the mode. Furthermore, there is no significant difference in the magnitude of the cross sections for the symmetric stretching and asymmetric stretching modes due to the close fundamental frequencies (see table 1).

The thermally averaged rate coefficient $\alpha_{v_i' \leftarrow v_i}(T)$ is obtained from the energy-dependent cross sections of equation (3)

$$\alpha_{v_i' \leftarrow v_i}(T) = \frac{8\pi}{(2\pi k_b T)^{\frac{3}{2}}} \int_0^\infty \sigma_{v_i' v_i}(E_{el}) e^{-\frac{E_{el}}{k_b T}} E_{el} \, dE_{el}, \quad (5)$$

where k_b is the Boltzmann constant and T is the temperature.

The rate coefficient is first calculated separately for singlet and triplet transitions and then the final rate coefficient is obtained taking into account the corresponding statistical weights: 1/4 for singlet and 3/4 for triplet. Figure 5 displays the spin- and thermally-averaged rate coefficients for (de-) excitation transitions between the three lowest vibrational states of the bending mode as an example.

Similarly to the previous studies [21, 22], for convenience of use, we fitted the numerical spin- and thermally-averaged rate coefficients to the following analytical formula

$$\alpha^{\text{fit}}_{v_i' \leftarrow v_i}(T) = \frac{1}{\sqrt{T}} e^{-\frac{\Delta_{v_i' \leftarrow v_i}}{T}} P^{\text{fit}}_{v_i' v_i}(x), \quad (6)$$

where

$$P^{\text{fit}}_{v_i' v_i}(x) = a_0 + a_1 x + a_2 x^2 \qquad \text{and} \qquad x = \ln(T). \quad (7)$$

The quantity $P^{\text{fit}}_{v_i' v_i}(x)$ is the (de-)excitation probability. It depends weakly on the scattering energy. The temperature in the above equation should be in kelvin to obtain rate coefficients in units of $cm^3\ s^{-1}$. In equation (6), $\Delta_{v_i' \leftarrow v_i}$ is the threshold energy defined as

$$\Delta_{v_i' \leftarrow v_i} = \begin{cases} E_{v_i'} - E_{v_i} > 0 & \text{for excitation,} \\ 0 & \text{for (de}-\text{)excitation.} \end{cases} \quad (8)$$

The numerically fitted values of coefficients $a_i (i = 0, 1, 2)$ for each individual transitions $v_i' \leftarrow v_i$ are listed in table 2. Figure 5 also demonstrates the fitted curves by equation (6). These curves are displayed in stars with same color for each transition obtained numerically. Evidently, the fitting curves exhibit a good agreement with that numerically obtained. The coefficient a_0 of the $1 \leftarrow 0$ transition for symmetric stretching mode is negative because the behavior of the cross section is not E_{el}^{-1} as shown in figure 4(b).

4. Uncertainty estimations

To our best knowledge, there exists no experimental or theoretical VE cross sections or rate coefficients data available for comparison with the present results. Hence, the uncertainty estimations for the theoretical model are very important to validate the present data. For an *ab initio* study like this one, uncertainties could and should be provided for intermediate quantities as well as for final calculated observables, such as excitation and ionization energies, potential energy surfaces, dipole moments, polarizabilities, etc.

From a point of view of an electro-static model potential for the electron-NO_2 collisions, the major contribution to the scattering amplitude for vibration excitation is expected to be due to variations of the permanent dipole moment and the polarizabilities of NO_2 along the normal mode coordinates. We do not use the model potential method in the study: the accuracy of the final cross sections depends on the accuracy of wave functions of the target and the scattering electron. The accuracy of computed wave functions cannot be compared with previous results directly. However, comparing the dipole moment, evaluated from wave functions of the target molecule, with the available accurate data can give an idea about the accuracy of computed wave functions used in the

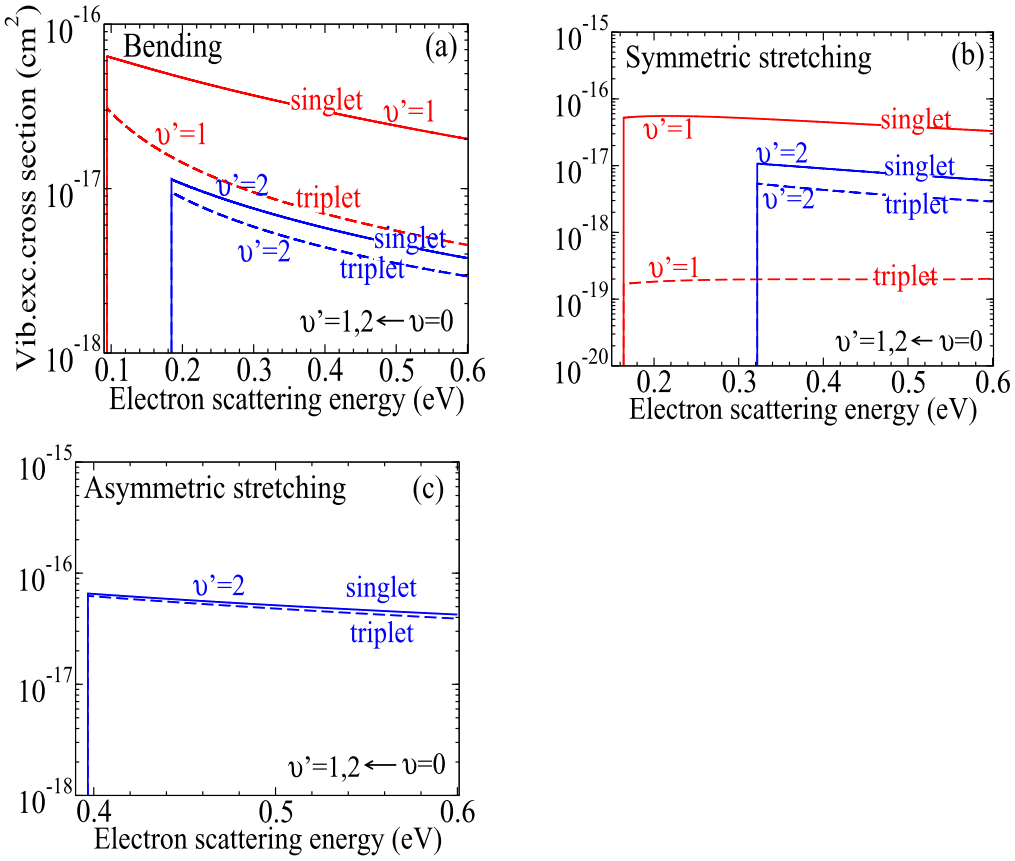

Figure 4. Calculated cross sections as functions of the electron scattering energy for the vibrational excitation of NO_2 being initially in the lowest vibrational state $v = 0$ for the three normal modes (see the text for detailed discussion): (a) cross sections for $v' = 1, 2 \leftarrow v = 0$ transitions for bending mode; (b) for symmetric stretching mode; (c) for asymmetric stretching mode.

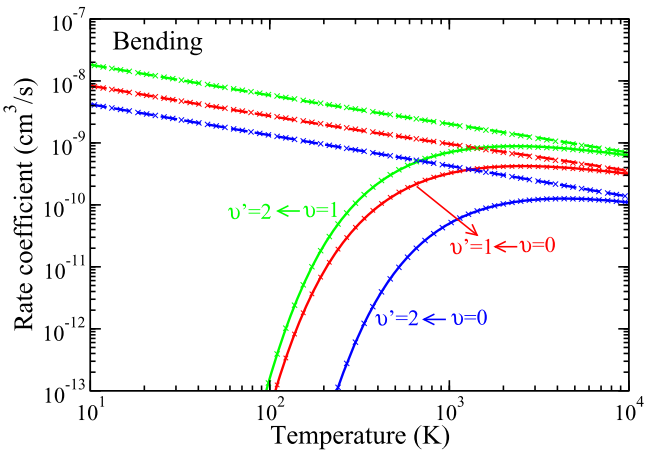

Figure 5. Spin- and thermally-averaged rate coefficients for (de-) excitation transitions between the three lowest vibrational states of the bending mode. Vibrational excitations are labeled by $\upsilon' \leftarrow \upsilon$. Corresponding de-excitations are shown by dashed lines of the same color. The figure also demonstrates the quality of the fit of equation (6): fitted curves are shown by stars with the same color for each transition.

R-matrix calculations and, correspondingly, about the accuracy of the final cross sections. Here, we investigate the stability of the dipole moment of target molecule as an example by performing a complete *R*-matrix calculation with different active spaces and basis sets and compare the results with experimental data. We carried out two set of computations: (1) using the CAS (referred here as CAS4) mentioned in section 2 and increasing the size of basis sets; (2) increasing the complete active space (CAS) with the `cc-pVTZ` basis set. The obtained results at the equilibrium geometry using the various parameters are illustrated in figure 6. As one can see in figure 6(a), the dipole moment approaches the experimental value 0.316 D when we increase the basis set. Evidently, the dipole moment obtained by `cc-pVTZ` basis set used in this study agrees with the experimental data very well. Augmented (`aug-`) basis sets are not used as they would significantly extend outside the *R*-matrix sphere. Figure 6(b) displays the variation of dipole moment as a function of different CAS's for the `cc-pVTZ` basis set. Obviously, the CAS used currently, i.e. CAS4 corresponds to the dipole moment closest to the experimental data. Therefore, we concluded that the target properties obtained by Quantemol-N are well converged and accurately represented. It might also be desirable to provide uncertainties for other intermediate quantities computed in collisional studies, such as eigenphase sums. These are also shown in figure 6, panel (c). As shown in the figure, the small shift observed in calculations with different CAS's indicates the convergence of the scattering data.

Another source of the uncertainty is the accuracy of the *S*-matrix derived from the UKRmol suite, when the dipole

Table 2. Parameters a_0, a_1 and a_2 of the polynomial $P^{\text{fit}}_{v_i' v_i}(x)$ of equations (6) and (7) between the three lowest vibrational states. The pairs of the final and initial vibrational levels for each normal mode are at the second line in each header of the three tables. The third line in each header gives the threshold energies $\Delta_{v_i' \leftarrow v_i}$ in equation (8). The $\Delta v = 1$ transitions for asymmetric stretching mode are forbidden by symmetry.

	Bending					
$v_i' \leftarrow v_i$	$1 \leftarrow 0$	$2 \leftarrow 0$	$0 \leftarrow 1$	$2 \leftarrow 1$	$0 \leftarrow 2$	$1 \leftarrow 2$
$\Delta_{v_i' \leftarrow v_i}$ (K)	1092	2142	0	1050	0	0
a_0	1.98×10^{-8}	1.25×10^{-8}	2.66×10^{-8}	4.33×10^{-8}	1.33×10^{-8}	5.75×10^{-8}
a_1	1.47×10^{-9}	2.17×10^{-10}	-4.13×10^{-10}	3.75×10^{-9}	6.17×10^{-12}	-2.96×10^{-10}
a_2	1.65×10^{-11}	-1.09×10^{-11}	1.40×10^{-10}	-1.03×10^{-10}	3.10×10^{-12}	1.67×10^{-10}
	Symmetric stretching					
$v_i' \leftarrow v_i$	$1 \leftarrow 0$	$2 \leftarrow 0$	$0 \leftarrow 1$	$2 \leftarrow 1$	$0 \leftarrow 2$	$1 \leftarrow 2$
$\Delta_{v_i' \leftarrow v_i}$ (K)	1904	3735	0	1831	0	0
a_0	-3.32×10^{-9}	1.48×10^{-8}	1.58×10^{-8}	2.92×10^{-8}	1.56×10^{-8}	5.79×10^{-8}
a_1	4.24×10^{-9}	2.46×10^{-10}	-9.05×10^{-10}	7.34×10^{-9}	1.77×10^{-11}	-5.71×10^{-10}
a_2	-4.28×10^{-11}	-1.35×10^{-10}	2.81×10^{-10}	-2.54×10^{-10}	1.84×10^{-12}	2.60×10^{-10}
	Asymmetric stretching					
$v_i' \leftarrow v_i$	$1 \leftarrow 0$	$2 \leftarrow 0$	$0 \leftarrow 1$	$2 \leftarrow 1$	$0 \leftarrow 2$	$1 \leftarrow 2$
$\Delta_{v_i' \leftarrow v_i}$ (K)	2346	4604	0	2257	0	0
a_0	—	2.03×10^{-7}	—	—	1.81×10^{-7}	—
a_1	—	-5.45×10^{-9}	—	—	3.63×10^{-10}	—
a_2	—	2.40×10^{-10}	—	—	-1.22×10^{-10}	—

Table 3. Coefficients from the curves fitting $|S_{l'\lambda',l\lambda}|^2 = \beta E^{\alpha}$ and $|\tilde{S}_{l'\lambda',l\lambda}|^2 = \beta' E^{\alpha'}$ (E is in eV).

	$\lvert S_{l'\lambda',l\lambda}\rvert^2 = \beta E^{\alpha}$		$\lvert \tilde{S}_{l'\lambda',l\lambda}\rvert^2 = \beta' E^{\alpha'}$	
$l'\lambda' \leftarrow l\lambda$	β	α	β'	α'
$00 \leftarrow 00$	1.00×10^{0}	1.82×10^{-3}	1.00×10^{0}	1.56×10^{-3}
$10 \leftarrow 00$	2.84×10^{-2}	6.40×10^{-2}	4.54×10^{-2}	1.86×10^{-1}
$20 \leftarrow 00$	4.21×10^{-5}	1.01×10^{-1}	1.98×10^{-5}	1.90×10^{-1}
$22 \leftarrow 00$	4.30×10^{-3}	9.34×10^{-1}	4.34×10^{-3}	9.34×10^{-1}
$20 \leftarrow 10$	4.07×10^{-3}	1.14×10^{-3}	8.01×10^{-3}	1.46×10^{-3}
$30 \leftarrow 20$	1.77×10^{-3}	7.61×10^{-4}	3.53×10^{-3}	3.28×10^{-4}
$40 \leftarrow 30$	9.84×10^{-4}	6.28×10^{-4}	1.96×10^{-3}	3.83×10^{-4}
$32 \leftarrow 00$	7.42×10^{-6}	1.06×10^{0}	1.05×10^{-6}	1.10×10^{0}
$42 \leftarrow 00$	2.43×10^{-9}	1.12×10^{0}	7.23×10^{-10}	7.50×10^{-1}
$44 \leftarrow 00$	1.25×10^{-7}	1.92×10^{0}	1.26×10^{-7}	1.92×10^{0}

term is included in the interaction. For the electron scattering by a nonpolar molecule, the electronic angular momenta l are decoupled at large distances from the target, such that l is a good quantum number for large separations between the electron and the molecule. However, for a dipolar molecule the electronic angular momenta l are coupled at long, as at short distances. The dipolar interaction exhibits the same long-range behavior as the centrifugal potential, thus, it is possible to combine the centrifugal and dipole interactions and obtain effective angular momentum. The Schrödinger equation for an electron in a dipole field is given by (in atomic units)

$$\left(-\frac{1}{2}\frac{\mathrm{d}^2}{\mathrm{d}r^2} + \left(\frac{\hat{L}^2}{2r^2} - \frac{D\cos\theta}{r^2}\right) - E\right)\psi = 0, \tag{9}$$

where $\hat{L}^2$ is the square of the orbital angular momentum, D is the dipole moment of NO_2, r and θ (polar angle) are the relevant spherical coordinates of the incident electron with respect to the center of mass of the target, E is the total energy of the system.

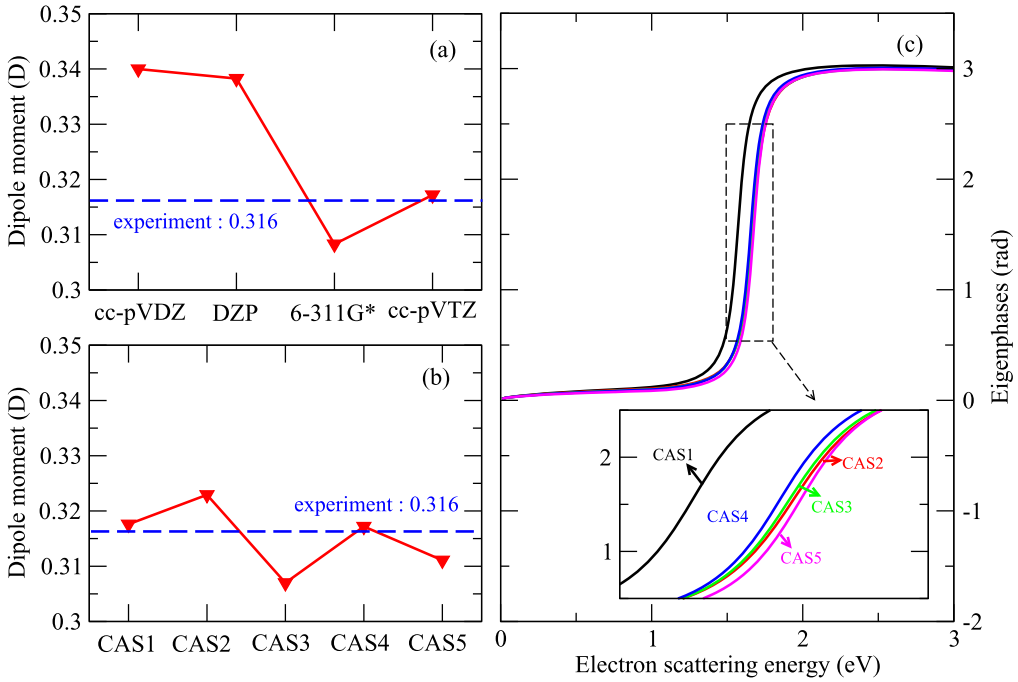

Figure 6. Variation of the computed permanent dipole moment of NO_2 versus different basis sets (panel (a)) and CAS (panel (b)). CAS1: 7 electrons are kept free in the active space including 7 orbitals; CAS2: 9 electrons are kept free in the active space including 8 orbitals; CAS3: 11 electrons are kept free in the active space including 9 orbitals; CAS4 (CAS used in this paper): 13 electrons are kept free in the active space including 10 orbitals; CAS5: 15 electrons are kept free in the active space including 11 orbitals. The blue dashed line indicates the experimental value of the dipole moment of [19]. (c) The eigenphase sums of scattering of the $^3B_1$ symmetry of the e^-–NO_2 complex as a function of the electron scattering energy for different CAS's. The inset enlarges the region where a sharper energy-dependence is observed around 1.6 eV corresponding to a resonance.

We find eigenvalues of the operator $\frac{\hat{L}^2}{2} - D\cos\theta$ and compute effective values of l. The eigenvectors of this operator are used to build the unitary matrix to transform the scattering matrix into the effective angular momentum representation. The values of the effective angular momentum l could be noninteger and even complex. On the next step, we fitted the obtained S-matrix elements (absolute values squared) before $|S_{l'\lambda',l\lambda}|^2$ and after $|\tilde{S}_{l'\lambda',l\lambda}|^2$ the unitary transformation with power law: $|S_{l'\lambda',l\lambda}|^2 = \beta E^{\alpha}$ and $|\tilde{S}_{l'\lambda',l\lambda}|^2 = \beta' E^{\alpha'}$, respectively, where α, β and α', β' are the fitted parameters. The obtained parameters are given in table 3. Figure 7 shows a few examples of scattering matrix elements of dominant channels ($\Delta l \leqslant 2$ and λ is zero) of the $^1A_1$ symmetry. The largest matrix element for the $00 \leftarrow 00$ transition is unchanged after the unitary transformation. It is the variation of this matrix element with respect to the normal coordinates that gives the largest contribution to the cross sections. Therefore, the uncoupling the partial-wave channels at large distances would not produce a significant change in the final cross sections. This also means that the coupling between partial waves induced by the permanent dipole moment of the target has a minor effect on the final cross sections.

Assuming that the order of magnitude of the VE cross sections is determined by the square of the derivatives of the permanent dipole moment and polarizabilities of the target with respect to the normal coordinates, and also assuming that the relative uncertainties of the derivatives are of the same order as the relative uncertainties of the dipole moment, we can estimate the uncertainty of the obtained cross sections with respect to the accuracy of the wave functions of the target. From panels (a) and (b) in figure 6, we estimate that the uncertainty in the dipole moment of NO_2 is less than 2%, producing the uncertainty in cross sections less than 4%. Another source of uncertainty in the final cross sections is due to the variation of the geometry-fixed scattering matrix with energy. The choice of the energy at which the scattering

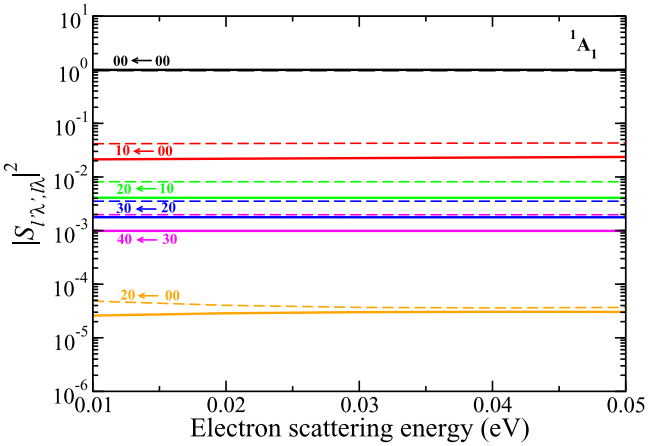

Figure 7. The figure compares selected values of the $^1A_1$ scattering matrix elements (absolute value squared) before (solid color lines) and after (dashed lines of the same color) the unitary transformation that eliminates the long-range dipolar coupling between asymptotic channels in the e^-–NO_2 scattering matrix in the body frame. See the detailed discussion in the text. Each curve is labeled at the left of the figure with the pair of indexes ($l'\lambda' \leftarrow l\lambda$), corresponding to the final channels and initial channel. The results for other irreps are not displayed but the situation is very similar to the $^1A_1$ symmetry.

matrix $S_{l'\lambda',l\lambda}(\boldsymbol{q})$ in equation (4) is computed produces the corresponding uncertainty. Figure 3 gives an idea about the energy variation of $S_{l'\lambda',l\lambda}(\boldsymbol{q})$. The largest components with $\Delta l = 0$ vary for about 3% over the energy interval of 0.4 eV. It gives an uncertainty in the cross sections of the order of 6%. No other significant uncertainty sources were identified. Therefore, the overall uncertainty of the present calculations seems to be below 10%.

5. Conclusions

This study reported the first theoretical results on VE and de-excitation of the NO_2 ($X\,^2A_1$) molecule in collisions with a low-energy electron. The calculation is performed using an approach that combines the normal mode approximation for the vibrational states of the target, the *R*-matrix method, and the vibrational frame transformation. Cross sections and spin- and thermally-averaged rate coefficients are obtained for excitation of all three NO_2 modes by one and two quanta from the ground vibrational level.

In addition, extensive uncertainty estimations were performed by changing the basis sets and orbital spaces in the *R*-matrix calculations. Converged results for the target properties and eigenphase sums demonstrated the validity of the obtained results. We expect that the data reported in the present study could be valuable in kinetic studies of low-temperature NO_2-containing plasma. Moreover, we expect that our approach will also work for other triatomic molecules such as SO_2 and O_3, which are also of atmospheric interest and have symmetry and electric properties similar to NO_2.

Acknowledgments

This work was supported by the China Scholarship Council, the Thomas Jefferson Fund of the Office for Science and Technology of the Embassy of France in the United States and the National Science Foundation, Grant No. PHY-1806915. It has also received funding from the program 'Accueil des chercheurs étrangers' of CentraleSupélec and 'Séjour à l'étranger 2019' of l'école doctorale INTERFACES of Université Paris-Saclay.

ORCID iDs

Hainan Liu https://orcid.org/0000-0003-2448-6052

References

[1] Shomali M, Opie D, Avasthi T and Trilling A 2015 *PLoS One* **10** e0130043
[2] Clough P and Thrush B A 1967 *Trans. Faraday Soc.* **63** 915–25
[3] Bernstein J A, Alexis N, Barnes C, Bernstein I L, Nel A, Peden D, Diaz-Sanchez D, Tarlo S M and Williams P B 2004 *J. Allergy Clin. Immunol.* **114** 1116–23
[4] Collin J 1959 *J. Chem. Phys.* **30** 1621–1621
[5] Kiser R W and Hisatsune I 1961 *J. Phys. Chem.* **65** 1444–6
[6] Stephan K, Helm H, Kim Y, Seykora G, Ramler J, Grössl M, Märk E and Märk T 1980 *J. Chem. Phys.* **73** 303–8
[7] Szmytkowski Maciag K and Krzysztofowicz A 1992 *Chem. Phys. Lett.* **190** 141–4
[8] Zecca A, Melissa R, Brusa R S and Karwasz G P 1999 *Phys. Lett.* A **257** 75–82
[9] Fox R 1960 *J. Chem. Phys.* **32** 285–7
[10] Rangwala S A, Krishnakumar E and Kumar S 2003 *Phys. Rev.* A **68** 052710
[11] Munjal H, Baluja K and Tennyson J 2009 *Phys. Rev.* A **79** 032712
[12] Ehrhardt H and Morgan L A 1994 *Electron Collisions with Molecules, Clusters, and Surfaces* (Berlin: Springer Science & Business Media) pp 47–62
[13] Benoit C and Abouaf R 1991 *Chem. Phys. Lett.* **177** 573–8
[14] Werner H, Knowles P, Knizia G and Manby W 2012 *Comput. Mol. Sci.* **2** 242
[15] Kendall R A, Dunning T H Jr and Harrison R J 1992 *J. Chem. Phys.* **96** 6796–806
[16] Johnson R D III 2019 NIST Computational Chemistry Comparison and Benchmark Database; NIST Standard Reference Database Number 101 (https://doi.org/10.18434/T47C7Z)
[17] Tennyson J 2010 *Phys. Rep.* **491** 29–76
[18] Tennyson J, Brown D B, Munro J J, Rozum I, Varambhia H N and Vinci N 2007 *J. Phys.: Conf. Ser.* **86** 012001
[19] Leonardi E, Petrongolo C, Hirsch G and Buenker R J 1996 *J. Chem. Phys.* **105** 9051–67
[20] Chang E and Fano U 1972 *Phys. Rev.* A **6** 173
[21] Kokoouline V, Faure A, Tennyson J and Greene C H 2010 *Mon. Not. R. Astron. Soc.* **405** 1195–202
[22] Ayouz M and Kokoouline V 2016 *Atoms* **4** 30